metals

MDPI

Article

Formation of Widmanstätten Ferrite and Grain Boundary Ferrite in a Hypereutectoid Pearlitic Steel

Sixin Zhao [1], Na Min [2,*] and Wei Li [3,4]

[1] R&D Center, Long Products Research Institute, Baoshan Iron & Steel Co Ltd., Shanghai 201900, China; zhaosixin@baosteel.com
[2] Laboratory for Microstructures, Shanghai University, Shanghai 200444, China
[3] Shanghai Key Laboratory of Materials Laser Processing and Modification, Shanghai Jiao Tong University, Shanghai 200240, China; weilee@sjtu.edu.cn
[4] School of Materials Science and Engineering, Shanghai Jiao Tong University, Shanghai 200240, China
* Correspondence: minnacy@shu.edu.cn

Abstract: Accompanied by the formation of pearlite, Widmanstätten ferrite (WF), grain boundary ferrite and cementite are often found to nucleate at the prior austenite grain boundary during isothermal heat treatment. A hypereutectoid pearlitic steel transformed isothermally at temperatures ranging from 607 to 707 °C was investigated to clarify the evolution of different phases. At 607 °C, WF grains, which had a Kurdjumov–Sachs orientation relationship with the remaining austenite, were found to be aligned with the grain boundary. At 707 °C, lath WF grains, which were arranged parallel to each other, were at a certain angle to the grain boundary. The formation of pearlite showed two-stage kinetics in the dilatometer curve, and the grain boundary's abnormal structure was suppressed.

Keywords: hypereutectoid pearlitic steel; Widmanstätten ferrite; Kurdjumov–Sachs orientation; grain boundary ferrite

Citation: Zhao, S.; Min, N.; Li, W. Formation of Widmanstätten Ferrite and Grain Boundary Ferrite in a Hypereutectoid Pearlitic Steel. *Metals* **2022**, *12*, 493. https://doi.org/10.3390/met12030493

Academic Editors: Alexander McLean and Francesca Borgioli

Received: 10 February 2022
Accepted: 9 March 2022
Published: 14 March 2022

1. Introduction

The eutectoid transformation of high carbon steels has aroused extensive attention because it renders a natural lamellar mixture of ferrite and cementite. The pearlitic microstructure in carbon steels is perhaps the most versatile of all man-made composites. Fully pearlitic steels are used in a number of important applications, such as high-strength wires, bridge cables and tee rails, etc. [1–3]. By heavily drawing full pearlitic steels into fine wires, significant strengths have been achieved, including extremely high strengths up to 7 GPa [4–6]. To cater to the engineers' appetites for strength, researchers have investigated high carbon steels [7,8]. However, when the carbon content is increased to higher than 0.8 wt.%, continuous grain boundary cementite can form, which may cause embrittlement after heavy cold drawing [9,10]. Some studies have pointed out that microalloying can impede grain boundary cementite formation. Han [11] indicated that the addition of vanadium and silicon can inhibit the formation a continuous cementite network. They proposed that the addition of silicon was determined to decrease the solubility of vanadium carbide particles in both austenite and ferrite by raising the carbon activity [12]. It also results in the occurrence of the grain boundary ferrite (GB-α) and WF coupled with discrete grain boundary cementite particles in hypereutectoid steels. Nevertheless, there are many studies reporting that GB-α forms along prior austenite grain boundaries [13,14], which causes delamination during the drawing of wires. Hillert [15] reported that the carbon content in austenite close to θ becomes lower than the Ae3 composition, leading to the nucleation of α. On the other hand, when hypereutectoid steels are transformed at a much lower temperature in the production of steel wire, the formation of GB-α was reported [12,16,17]. They investigated the isothermal transformation of hypereuctoid steels and found that

the volume fraction of GB-α decreases with increasing transformation temperature, but increases remarkably in the transformation at 700 °C due to the formation of proeutectoid θ along the γ grain boundary initially and induces the nucleation of GB-α at the θ/γ interface [16]. The grain boundary of ferrite demonstrated a near-Kurdjumov–Sachs (K–S) orientation in the transformation at low temperature when cementite nucleation at the ferrite/austenite boundary was suppressed [16]. Therefore, the carbon content, cooling rate and isothermal transformation temperature are important factors which determine the grain boundary ferrite nucleation and formation.

Although the existence of this abnormal ferrite has subsequently been repeatedly confirmed in alloyed eutectoid steel and hypereutectoid steels, it is not fully understood whether GB-α forms before or after the nucleation of the pearlite. Therefore, the present study aims to provide more direct experimental evidence of microstructure characterization of grain boundary ferrite in high carbon steels and to clarify the formation mechanism of abnormal α.

2. Materials and Methods

A hypereutectoid steel with the composition of Fe-0.92wt.%C-1.00wt.%Si and other microalloy elements was prepared. The isothermal transformation of austenite was analyzed using a high-resolution dilatometer (DIL805A). Cylindrical dilatometric machined specimens (4 mm in diameter and 10 mm in length) were used for these tests. The change in length of the specimens was transmitted via an amorphous silica pushrod. Cooling was carried out by blowing a jet of helium gas directly onto the specimen surface. The helium flow rate during cooling was controlled by a proportional servo-valve. The heating and cooling devices of this dilatometer are efficient in controlling the temperature and holding time of isothermal treatments and performing fast cooling in the quenching processes. The specimens were austenited at 960 °C for 15 min and subsequently, isothermally transformed at 607 and 707 °C for 5, 10, 15 and 180 s, respectively.

Microstructures of the transformed specimens were observed by means of optical microscopy, scanning transmission electron microscopy (SEM) and transmission electron microscopy (TEM), respectively. Volume fractions of pearlite were determined by point counting in optical micrographs. For optical and SEM observation, 5% nitric acid alcohol solution was used for etching. Thin foils were prepared for TEM and transmission Kikuchi diffraction (TKD) observations by electro-polishing using Struers (Tenupol-5) (Struers Inc., Westlake, OH, USA) equipment at -20°/30 V. The electrolyte consisted of 7% perchloric acid and 93% ethanol. TEM observation was performed by using JOEL JEM-2100F operated at 200 kV (JEOL (JP) Ltd., Tokyo, Japan). A scanning electron microscope (SEM) (TESCAN MIRA3) equipped with an electron back-scatter diffraction (EBSD) detector was used to analyze strain distribution and phase features by the transmission Kikuchi diffraction (TKD) technique (TESCAN Ltd., Kohoutovice, Czech Republic). A total of the EBSD map per sample was acquired at an accelerating voltage of 20 kV with an aperture size of 120 µm. The step size was set at 0.2 µm. The acquisition speed per point was 970 Hz and the time needed to acquire an entire map was 20 min. The resulting indexing rate was 95%.

3. Results and Discussion

Figure 1 illustrates the real-time length changes from the dilatometer for steel sample quenching at 960 °C and isothermal holding at 607 and 707 °C. The sigmoid extension curves with duration of time are rational corresponding to the volume expansion of both $\gamma \rightarrow \alpha$ and $\gamma \rightarrow \alpha + \theta$ phase transitions. It is apparent that the transformation at 607 °C reached the saturated state much faster than that at 707 °C due to the larger driving force from the higher degree of cooling for the phase transition. Meanwhile, the undulating curve at 707 °C revealed two-stage kinetics, which is not observed for the curve of 607 °C. To clarify the cause of this behavior, interrupted quenching samples after isothermal treatment for the short and long term were prepared and observed. As shown in Figure 1a, a pearlite colony was found after 5 s in the microstructure, and it is surrounded by martensite, which formed

from quenching of the unstable austenite. At the pearlite/martensite boundaries, some inclined lath microstructures of Widmanstätten ferrite are observed. However, such a lath structure disappeared when the isothermal time increased to 180 s, and grain boundary ferrite and degenerated pearlite containing globular cementite particles were observed. For the samples undergoing isothermal heat treatment at 707 °C for 5 s, shown in Figure 1f, saw tooth structures parallel to each other are found rooted in the pearlite/martensite interface. It is worth noting that the pearlite colony stopped growing when it reached a diameter of about 25 μm by comparing the microstructures of isothermal heat-treated samples for 10 to 15 s. The normal pearlite started growth again after 100 s, which corresponds to the dilatometer curve. When the transformation lasted for 300 s, the full lamellar microstructures formed but with few GB-α at the prior austenite grain boundary, and no apparent GB-α or GB-θ were found at the prior austenite grain boundaries.

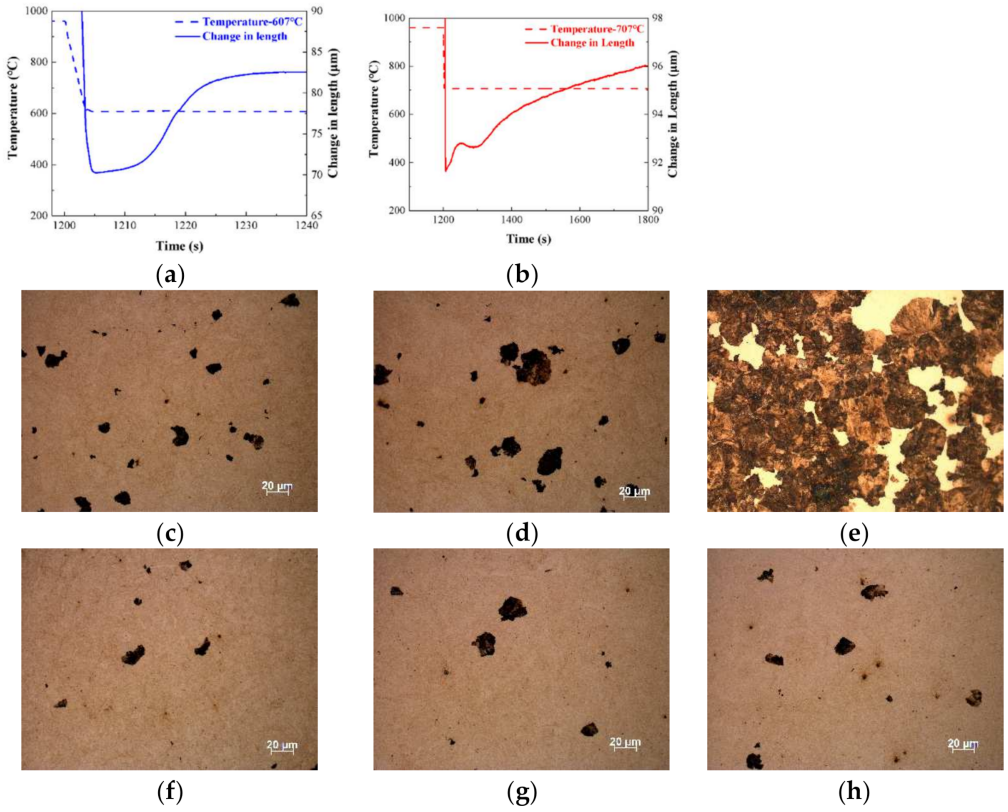

Figure 1. Dilatometer curves of isothermal transformation at 607 °C (**a**) and 707 °C (**b**); OM diagram of short-time isothermal quenching structure. (**c**) 607 °C—5 s; (**d**) 607 °C—10 s; (**e**) 607 °C—15 s; (**f**) 707 °C—5 s; (**g**) 707 °C—10 s; (**h**) 707 °C—15 s.

As shown in Figure 2, it also can be observed that most of the WF nucleates at the original γ-grain boundary and grows into the other γ grains. The size of WF reaches about 2 μm. With the increase in isothermal time, lamellar pearlite gradually engulfs γ grains, and the volume fraction of WF decreases, as shown in Figure 2b,d. Compared to 607 °C, a larger size and greater volume fraction of WF was found in front of the GB-θ at 707 °C. Therefore, ferrite nucleation from the prior austenitic grain boundaries is preferred with higher temperature due to the sufficient carbon diffusion and much less free energy change of 50 J/mol compared to the cooperative growth of lamellar pearlite [18]. However, the growth of WF is inhibited by the subsequent formation of pearlite, due to the accumulation of carbon in the frontier of WF and cementite forming easily, leading to a pearlite colony. Chairuangsri and Edmonds proved that the growth of GB-α is accompanied with carbon rejection into the γ grain and even diffusing through α from the GB-α/γ interface to the GB-α/θ interface [19]. As the solubility of carbon in ferrite is two orders lower than that in

austenite, the transformation is accompanied by a carbon enrichment of the austenite. θ at the interface between pearlite and GB-α can coarsen due to the carbon supply, leading to the formation of GB/θ. However, both the body diffusion of carbon in austenite and the driving force constrained the continuous growth of both ferrite and pearlite at this temperature. Therefore, the length extension of the dilatometer at 707 °C stagnates until the normal nucleation starts after 100 s.

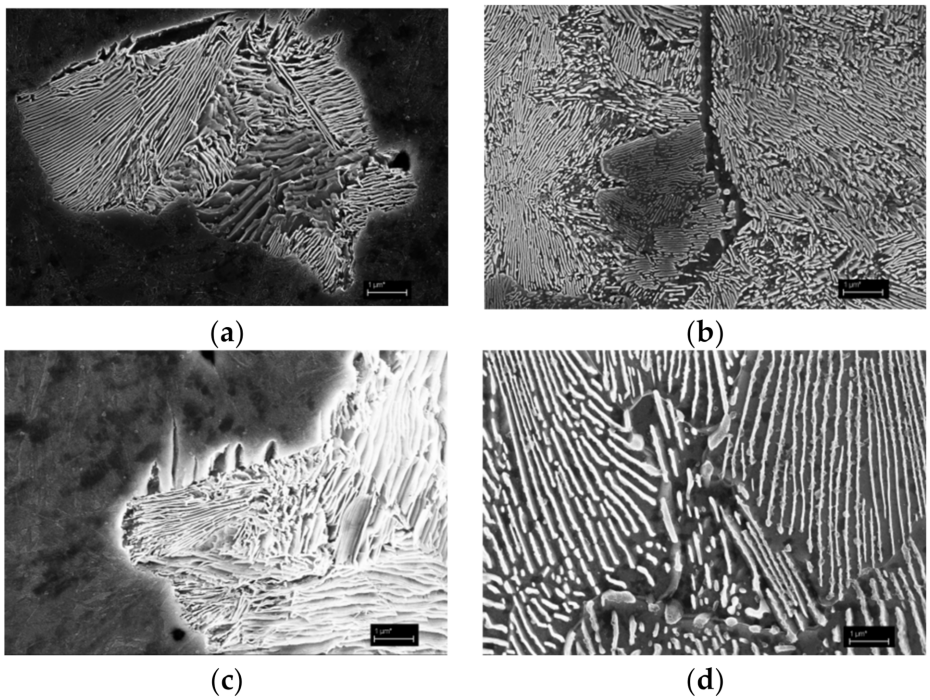

Figure 2. SEM microstructure near the grain boundary in the specimens at various temperature and times: (**a**) 607 °C—5 s; (**b**) 607 °C—180 s; (**c**) 707 °C—5 s; (**d**) 707 °C—300 s.

Figure 3 shows the transmission Kikuchi diffraction (TKD) results of the sample transformed at 607 °C for 15 s. Lath Widmanstätten ferrite from the prior austenite grain boundary was found to be aligned with the grain boundary. The immature morphology of WF compared to that at 707 °C is caused by the slower body diffusion of carbon and easy nucleation and growth of pearlite. The WF showed good Kurdjumov–Sachs (K–S) orientation with the two adjacent remaining austenites because the displacive transformation is kinetically favored at a lower transformation temperature and the coherent interface formed easily even without diffusion. Similar to the findings of Miyamoto [11], the GB-α hold near K–S orientation with one of the prior austenite grain boundaries and the pearlite grows from the other side and had no K–S orientation. Moreover, the GB-α in our study shared the same orientation of the lath WF and continually grows into a pearlite colony. Therefore, WF, GB-α and adjacent pearlite ferrite have a similar orientation, as shown in Figure 3b. The phase map in Figure 3c shows that the cementite coarsens to form a lath shape. Figure 4a is a TEM bright field (BF) image showing the orientation relationship of WF and the original γ at 707 °C for 15 s. The dark field (DF) image of the marked area in Figure 4a for the ferrite phase is shown in Figure 4b, exhibiting WF distribution. As can be seen from Figure 4c, the WF/γ OR is identified as Kurdjumov–Sachs (K–S) OR. It is demonstrated that the pearlite θ formed adjacently due to the carbon supply from the WF.

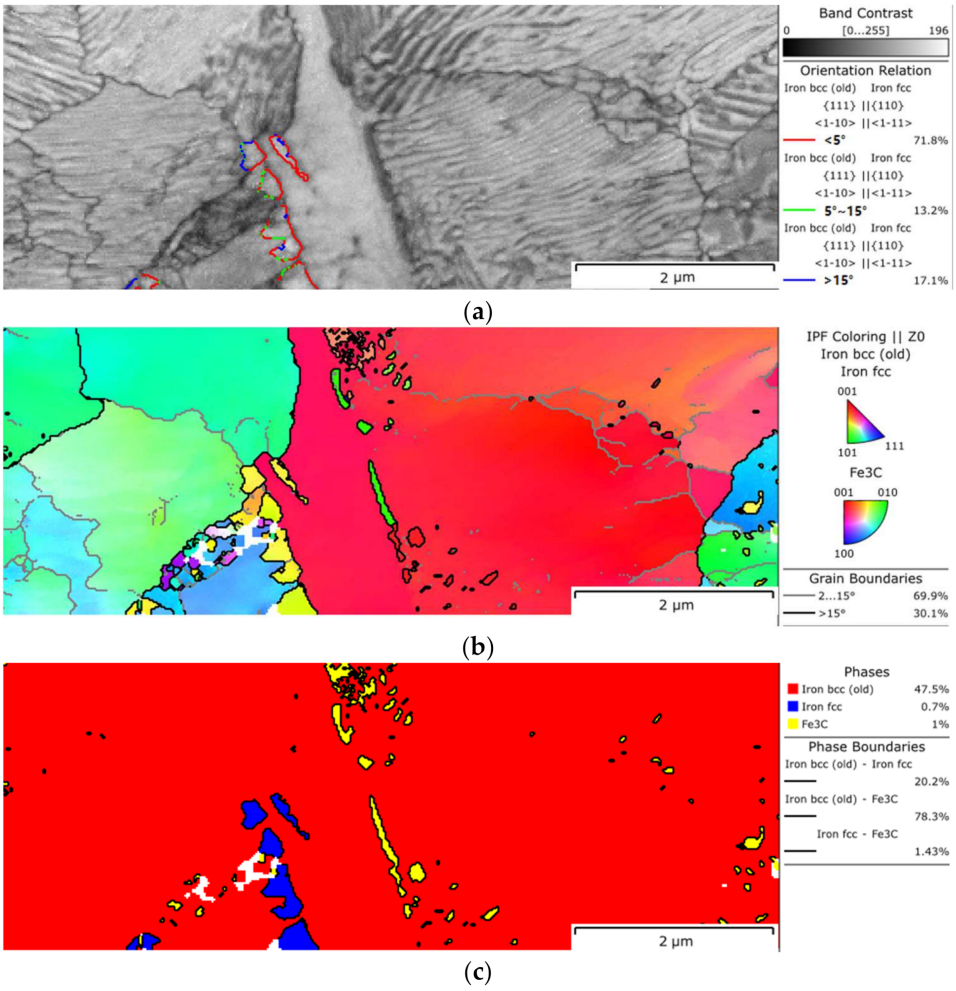

Figure 3. Microstructural analysis of sample transformed at 607 °C for 15 s by TKD analysis: (**a**) SEM image and K–S orientation deviation (white, 0°–5°; yellow, 5°–15°; green, >15°) and (**b**) corresponding orientation map; (**c**) corresponding phase map.

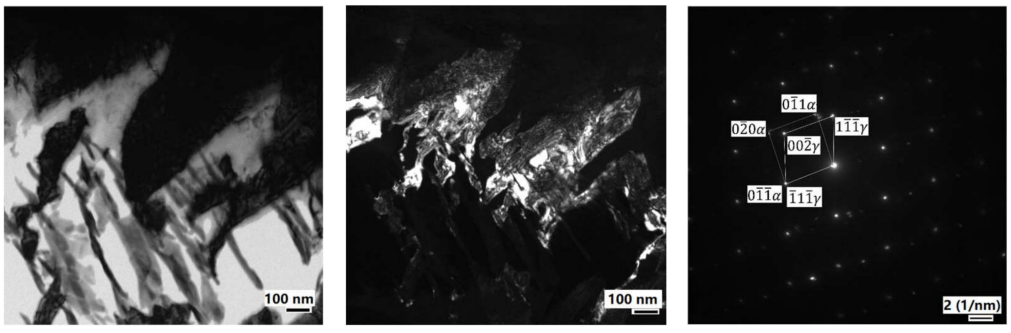

Figure 4. TEM microstructures of sample transformed at 707 °C for 15 s: (**a**) Bright field image; (**b**) selected area diffraction pattern showing the Kurdjumov–Sachs orientation of α/γ; (**c**) dark field image of WF.

The observation indicates that ferrite starts to form at the γ phase boundary. It was found that in the initial isothermal transformation, isothermally needle-like WF is arranged in parallel, and is at a certain angle from the grain boundary, in which it holds good Kurdjumov–Sachs orientation with the remaining austenite. At 707 °C, the volume fraction of grain boundary abnormal structures is suppressed mostly due to the adjacent pearlite

nucleation. Both the diffusion of carbon and the chemical driving force at this temperature constrained the continuous growth of the ferrite and pearlite [20]. It is interesting that the pearlite showed two-stage kinetics, and this may be influenced by the addition of silicon. At 607 °C, the coherent interfaces between austenite (γ) and ferrite (α) become dominant due to the limitation of the atomic mobility. Laths of ferrite grow from the grain boundary WF on the side of the coherent boundary with a Kurdjumov–Sachs relationship constituting the GB-α. The acceleration of pearlite transformation can effectively inhibit WF growth, and the addition of silicon is effective in the $\gamma \rightarrow \alpha$ and $\gamma \rightarrow \alpha + \theta$ kinetics and beneficial to suppress GB-θ formation.

4. Conclusions

Hypereutectoid steels were isothermally transformed at temperatures ranging from 607 to 707 °C, and GB-α, Gb-θ and WF microstructures near prior γ grain boundaries were investigated. The results are as follows:

1. WF laths arranged parallel and at a certain angle from with the original γ-grain boundary, accompanied by the formation of ferrite and pearlite at 607 °C. The WF, GB-α and adjacent pearlite ferrite have a K–S orientation due to the coherent interface being able to move displacively at lower transformation temperatures.
2. Two-stage pearlite kinetics was found at 707 °C. Meanwhile, grain boundary abnormal structures are suppressed at 707 °C, which is attributed to the suppression of the formation of grain boundary cementite, and thus is beneficial to obtain a balanced pearlite lamellar structure.

Author Contributions: Conceptualization, S.Z., W.L. and N.M.; methodology, N.M.; software, S.Z.; validation, S.Z., W.L. and N.M.; investigation, S.Z.; resources, S.Z. and N.M.; data curation, S.Z. and N.M.; writing—original draft preparation, S.Z.; writing—review and editing, S.Z., W.L. and N.M.; visualization, S.Z.; supervision, N.M.; project administration, N.M.; funding acquisition, S.Z., W.L. and N.M. All authors have read and agreed to the published version of the manuscript.

Funding: This research was funded by the National Natural Science Foundation of China, grant number 52071209.

Institutional Review Board Statement: Not applicable.

Informed Consent Statement: Not applicable.

Data Availability Statement: The data presented in this study are available on request from the corresponding author.

Acknowledgments: Na Min is grateful to Professor Ke Han for his useful comments during his reading of the final text.

Conflicts of Interest: The authors declare that they have no known competing financial interests or personal relationships that could have appeared to influence the work reported in this paper.

References

1. Baek, H.M.; Hwang, S.K.; Joo, H.S.; Im, Y.Y.; Son, I.H.; Bae, C.M. The effect of a non-circular drawing sequence on delamination characteristics of pearlitic steel wire. *Mater. Des.* **2014**, *62*, 137–148.
2. Maruyama, N.; Tarui, T.; Tashiro, H. Atom probe study on the ductility of drawn pearlitic steels. *Scr. Mater.* **2002**, *46*, 599–603. [CrossRef]
3. Jafari, M.; Bang, C.W.; Han, J.C.; Kim, K.M.; Na, S.H.; Park, C.G.; Lee, B.J. Evolution of microstructure and tensile properties of cold drawn hyper-eutectoid steel wires during post-deformation annealing. *J. Mater. Sci. Technol.* **2020**, *41*, 1–11.
4. Li, Y.J.; Choi, P.P.; Goto, S.; Borchers, C.; Raabe, D.; Kirchheim, R. Evolution of strength and microstructure during annealing of heavily cold-drawn 6.3 GPa hypereutectoid pearlitic steel wire. *Acta Mater.* **2012**, *60*, 4005–4016.
5. Li, Y.J.; Raabe, D.; Herbig, M.; Choi, P.P.; Goto, S.; Kostka, A.; Yarits, H.; Borchers, C.; Kirchheim, R. Segregation Stabilizes Nanocrystalline Bulk Steel with Near Theoretical Strength. *Phys. Rev. Lett.* **2014**, *113*, 106104. [CrossRef] [PubMed]
6. Li, Y.J.; Choi, P.; Borchers, C.; Westerkamp, S.; Goto, S.; Raabe, D.; Kirchheim, R. Atomic-scale mechanisms of deformation-induced cementite decomposition in pearlite. *Acta Mater.* **2011**, *59*, 3965–3977.

7. Lesuer, D.R.; Syn, C.K.; Sherby, O.D. Influence of severe plastic deformation on the structure and properties of ultrahigh-carbon steel wire. In *Investigations and Applications of Severe Plastic Deformation*; Lowe, T.C., Valiev, R.Z., Eds.; Kluwer Academic Publishers: Boston, MA, USA, 2000; pp. 357–366.
8. Taleff, E.M.; Syn, C.K.; Lesuer, D.R.; Sherby, O.D. Pearlite in ultrahigh carbon steels: Heat treatments and mechanical properties. *Metall. Mater. Trans. A* **1996**, *27*, 111–118.
9. Carsi, M.; Penalba, F.; Ruano, O.A.; Sherby, O.D. High strain rate torsional behavior of an ultrahigh carbon steel (1.8 Pct C-1.6 Pct Al) at elevated temperature. *Metall. Mater. Trans. A* **1997**, *28*, 1913–1920. [CrossRef]
10. Park, K.T.; Cho, S.K.; Choi, J.K. Pearlite morphology in the hypereutectoid steels. *Scr. Mater.* **1997**, *37*, 661–666. [CrossRef]
11. Han, K.; Edmonds, D.V.; Smith, G.D.W. Optimization of mechanical properties of high-carbon pearlitic steels with Si and V additions. *Metall. Mater. Trans. A* **2001**, *32*, 1313–1324. [CrossRef]
12. Han, K.; Mottishaw, T.D.; Smith, G.D.W.; Edmonds, D.V. Effects of vanadium addition on nucleation and growth of pearlite in high carbon steel. *Mater. Sci. Tech.* **1994**, *10*, 955–963. [CrossRef]
13. Shimizu, K.; Kawabe, N. Size dependence of delamination of high-carbon steel wire. *ISIJ Int.* **2001**, *41*, 183–191. [CrossRef]
14. Oki, Y.; Ibarak, N.; Ochiai, K.; Minamida, T.; Makii, K. Microstructure influence on ultra high tensile steel cord filament delamination. *Kobe Steel Eng. Rep.* **2000**, *50*, 37–40.
15. Hillert, M. *The Formation of Pearlite*; Interscience: New York, NY, USA, 1962; p. 197.
16. Miyamoto, G.; Karube, Y.; Furuhara, T. Formation of grain boundary ferrite in eutectoid and hypereutectoid pearlitic steels. *Acta Mater.* **2016**, *103*, 370–381. [CrossRef]
17. Nagao, M.; Yaguchi, H.; Ibaraki, N.; Ochiai, K. Suppression of secondary ferrite formation by boron addition in high carbon steel wires. *Tetsu-to-Hagane* **2003**, *89*, 329–334. [CrossRef]
18. Bhadeshi, H.; Honeycombe, R. *Steels: Microstructure and Properties*; Butterworth-Heinemann: Amsterdam, The Netherlands, 2017; pp. 203–216.
19. Chairuangsri, T.; Edmonds, D.V. Abnormal ferrite in hyper-eutectoid steels. *Acta Mater.* **2000**, *48*, 1581–1591. [CrossRef]
20. Offerman, S.E.; Van Dijk, N.H.; Sietsma, J.; Grigull, S.; Lauridsen, E.M.; Margulies, L.; Poulsen, H.F.; Rekveldt, M.T.; Zwaag, S.V.D. Grain nucleation and growth during phase transformations. *Science* **2002**, *298*, 1003–1005. [CrossRef] [PubMed]